International Journal of Nanomedicine

Dovepress
open access to scientific and medical research

Open Access Full Text Article

ORIGINAL RESEARCH

Modulation of Tumor Hypoxia by pH-Responsive Liposomes to Inhibit Mitochondrial Respiration for Enhancing Sonodynamic Therapy

This article was published in the following Dove Press journal:
International Journal of Nanomedicine

Nan Zhang[1,*]
Yang Tan[1,*]
Liwei Yan[2]
Chunyang Zhang[1]
Ming Xu[1]
Huanling Guo[1]
Bowen Zhuang[1]
Luyao Zhou[1]
Xiaoyan Xie[1]

[1]Department of Medical Ultrasonics, The First Affiliated Hospital of Sun Yat-sen University, Guangzhou, Guangdong 510080, People's Republic of China; [2]Department of Microsurgery and Orthopedic Trauma, The First Affiliated Hospital of Sun Yat-sen University, Guangzhou, Guangdong 510080, People's Republic of China

*These authors contributed equally to this work

Background and Purpose: Sonodynamic therapy (SDT) has been widely used for the noninvasive treatment of solid tumors, but the hypoxic tumor microenvironment limits its therapeutic effect. The current methods of reoxygenation to enhance SDT have limitations, prompting reconsideration of the design of therapeutic approaches. Here, we developed a tumor microenvironment-responsive nanoplatform by reducing oxygen consumption to overcome hypoxia-induced resistance to cancer therapy.

Methods: A pH-responsive drug-loaded liposome (MI-PEOz-lip) was prepared and used to reduce oxygen consumption, attenuating hypoxia-induced resistance to SDT and thereby improving therapeutic efficiency. Photoacoustic imaging (PAI) and fluorescence imaging (FI) of MI-PEOz-lip were evaluated in vitro and in breast xenograft tumor models. The pH-sensitive functionality of MI-PEOz-lip was applied for pH-triggered cargo release, and its capacity was evaluated. The MI-PEOz-lip-mediated SDT effect was compared with other treatments in vivo.

Results: MI-PEOz-lip was demonstrated to specifically accumulate in tumors. Metformin molecules in liposomes selectively accumulate in tumors by pH-responsive drug release to inhibit the mitochondrial respiratory chain while releasing IR780 to the tumor area. These pH-responsive liposomes demonstrated PAI and FI imaging capabilities in vitro and in vivo, providing potential for treatment guidance and monitoring. In particular, the prepared MI-PEOz-lip combined with ultrasound irradiation effectively inhibited breast tumors by producing toxic reactive singlet oxygen species (ROS), while the introduction of metformin inhibited mitochondrial respiration and reduced tumor oxygen consumption, resulting in excellent sonodynamic therapy performance compared with other treatments.

Conclusion: In this study, we present a novel strategy to achieve high therapeutic efficacy of SDT by the rational design of multifunctional nanoplatforms. This work provides a new strategy that can solve the current problems of inefficient oxygen delivery strategies and weaken resistance to various oxygen-dependent therapies.

Keywords: sonodynamic therapy, pH-responsive liposomes, tumor hypoxia relief, metformin, nanomedicine

Introduction

[1–3] Photodynamic therapy (PDT) utilizes reactive oxygen species (ROS) generated from a light-activated photosensitizer to damage cancer cells[4] and is a conventional clinical approach used for the treatment of dermatoma and other tumors.[5,6] However, it is often limited by the poor penetration capability of light through human tissue and is suitable only for superficial lesions. Sonodynamic therapy

Correspondence: Xiaoyan Xie
Department of Medical Ultrasonics, The First Affiliated Hospital of Sun Yat-sen University, Guangzhou 510080, People's Republic of China
Tel/ Fax +86-20-87765183
Email xiexyan@mail.sysu.edu.cn

submit your manuscript | www.dovepress.com
DovePress
http://doi.org/10.2147/IJN.S256038

(SDT) functions by a similar antitumor process and is emerging as an alternative to the more established treatment.[7] Compared with light, ultrasound (US) has the advantages of minimal invasiveness and deeper penetration but also changes the permeability of the cell membrane and stimulates the diffusion process of the cell semipermeable membrane.[8] Furthermore, it could be used to control the release of drugs and promote the penetration of additional nanoparticles or drugs into the tumor center through the cavitation effect.[9,10] However, up to 50–60% of advanced solid tumors exhibit high heterogeneity, leading to a hypoxic microenvironment, which limits the efficacy of SDT.

To ameliorate the hypoxic environment and enhance the therapeutic effect of SDT, several different strategies have recently been exploited,[11–15] such as directly providing more oxygen to tumor tissue by using perfluorocarbon-based oxygen carriers or transporting hydrogen peroxide catalysts to promote the reaction of endogenous H_2O_2 to generate oxygen.[16–19] These approaches could only temporarily alleviate hypoxia in the tumor[20] because of oxygen leakage during delivery and[13,14,18,19,21] the low efficiency of oxygen production during the reaction. As an alternative to delivering oxygen to the tumor, reducing oxygen consumption has received considerable attention because this approach can effectively eliminate hypoxia in sparsely vascularized areas by reducing the partial pressure of oxygen gradient in tumor tissue, further decreasing the resistance to various oxygen-dependent therapies.[22,23] It is worth noting that the principal function of mitochondrial-related oxidative phosphorylation (OXPHOS) is to generate energy by consuming oxygen.[24–26] Therefore, we believe that the inhibition of OXPHOS activity can effectively reduce oxygen consumption and prevent it from developing into hypoxia.

The antihyperglycemic agent metformin is an FDA-approved drug that has been shown to act as an effective respiratory inhibitor by directly inhibiting the activity of mitochondrial complex I. In 2013,[27] Zannella demonstrated that the intraperitoneal administration of free metformin could effectively reduce the tumor oxygen consumption rate and significantly improve the effects of radiotherapy on mouse xenografts. Nonetheless,[28] the conventional drug carrier usually releases the drug slowly, resulting in a low drug concentration in the tumor area and unsatisfactory therapeutic effects. In order to effectively exert a therapeutic effect, there is still a demand for drug delivery system that promotes drug concentration to rapidly reach the treatment window in tumor tissue.[29–31] A stimuli-responsive carrier system, especially a pH-responsive liposome, enables the active triggering of drug release that could control its local concentration within the therapeutic window. Therefore, pH-responsive liposomes can effectively release drugs and sonosensitizers in the acidic tumor tissue to alleviate tumor hypoxia and improve SDT.

In this study, we chose MDA-MB-231 breast cancer solid tumors as a treatment model because irregular cancer cells proliferate at the tumor periphery and limit the diffusion of oxygen into the deep layers of tumors, thereby forming local hypoxia as well as acidic environment. We herein successfully constructed pH-responsive drug-loaded liposomes to reduce oxygen consumption, attenuate hypoxia-induced resistance to SDT, and improve the SDT efficiency of breast cancer. Moreover, this liposome could act as a contrast agent for photoacoustic imaging (PAI) and fluorescence imaging (FI), providing guidance for the subsequent SDT. We chose IR780 as the sonosensitizer and antihyperglycemic drug metformin as the SDT enhancer, both of which were encapsulated by pH-responsive phospholipids to form liposomes (MI-PEOz-lip) to indicate that metformin activity enhanced the therapeutic effect of IR780-mediated SDT. Due to the enhanced permeability and retention (EPR) effect, intravenous infusion of MI-PEOz-lip could effectively deliver the drugs to the hypoxic sites of the tumors and release metformin in response to the acidic tumor tissue, thereby quickly achieving a concentration in the therapeutic window to reduce the oxygen consumption by interfering with the normal energy metabolism process and further enhancing the sensitivity of the sensitizer to produce ROS after US irradiation. As a result, an increasing number of cancer cells were killed, and tumors in mice were significantly reduced. Our research proposes a very simple and safe strategy that can solve the current problems of inefficient oxygen delivery strategies and weaken resistance to various oxygen-dependent therapies. Due to its excellent biocompatibility, this technology holds great clinical promise.

Materials and Methods

Materials

The lipids dipalmitoyl-sn-glycero-3-phosphocholine (DPPC), 1,2-distearoyl-sn-glycero-3-phosphoethanolamine-N-[methoxy (polyethylene glycol)-2000] (DSPE-PEG2000) and cholesterol were purchased from Avanti Polar Lipids, Inc. (Alabaster, AL, USA). DSPE-PEOz2000 was purchased

from Ruixi Biological Technology (Xi'an, Shanxi, China). IR780 iodide and metformin were purchased from Aladdin (Shanghai, China) and Sigma-Aldrich (St. Louis, Missouri, USA), respectively. Cell Counting Kit-8 (CCK-8) was purchased from Meilunbio® (Dalian, Liaoning, China). 2-(4-Amidino-phenyl)-6-indolecarbamidinedihydrochloride (DAPI), 1,3-diphenylisobenzofuran (DPBF) and 2′,7′-dichlorodihydrofluorescein diacetate (DCFH-DA) were obtained from Beyotime Technology (Shanghai, China). Deionized water was obtained from Millipore water purification systems. All reagents and solvents used in this subject were purchased commercially and used without further purification unless specifically stated in the instructions.

Synthesis of MI-PEOz-Lip

MI-PEOz-lip was synthesized by dissolving 12 mg of DPPC, 4 mg of cholesterol, 4 mg of DSPE-PEOz, and 1 mg of IR780 in 5 mL of chloroform in a flask. The solution was then volatilized completely by rotary evaporation in a water bath at 60°C. After the lipid membrane was formed, 500 μL of metformin solution (10 mg/mL) was added, and the mixture was sonicated for 0.5 h at 60°C. The suspension was strained 40 times through 400nm and 200 nm filters, and the IR780-loaded phospholipids formed liposomes with metformin aqueous solution in the core. The final MI-PEOz-lip product was purified using a G-50 Sephadex column. Metformin- and IR780-loaded liposomes (MI-PEG-lip, without pH-responsive phospholipids), IR780-loaded pH-sensitive liposomes (IR780-PEOz-lip) and IR780-loaded liposomes (IR780-lip) were fabricated according to the same procedure.

Characterization of MI-PEOz-Lip

The morphology of MI-PEOz-lip was analyzed by a transmission electron microscope (TEM, JEOL, JEM-2100F, Tokyo, Japan). The sizes and zeta potentials of MI-PEOz-lip and MI-PEG-lip were measured using a laser particle size analyzer system (Malvern Panalytical, Zeta SIZER 3000HS, Malvern, UK), and UV-vis-NIR spectra of metformin, IR780 and MI-PEOz-lip were obtained using a spectroscope (Shimadzu, UV-2550, Kyoto, Japan) at room temperature. To further evaluate the influence of pH, the morphology of MI-PEOz-lip in the acidic solution after 3 h was analyzed by a transmission electron microscope. Then, the size and zeta potentials of MI-PEOz-lip and MI-PEG-lip under the same conditions were analyzed by a laser particle size analyzer system. The standard concentration curve of the free metformin and IR780 solution were measured to determine the amount of metformin and IR780 encapsulated into liposomes. The concentration of metformin and IR780 were measured by using a high-performance liquid chromatography (HPLC) and UV–vis spectrometer method, respectively. The entrapment efficiency was calculated by the following formulas:

Metformin entrapment efficiency (%) = (Mass of metformin in composite liposomes/Total metformin inputs) × 100%

IR780 entrapment efficiency (%) = (Mass of IR780 in composite liposomes/Total IR780 inputs) × 100%

The corresponding formulation (0.25 mg/mL metformin and 0.05mg/mL IR780) was used for subsequent experiments. To investigate the metformin release profiles at different pH values, samples of the same MI-PEOz-lip and MI-PEG-lip solutions (1 mL) were dispersed in pH 5.5, pH 6.5, and pH 7.4 buffer solutions (20 mL), dialyzed against a 100 kDa MWCO dialysis bag, and rotated at 37°C and 100 rpm. At different time intervals, 1 mL of the dialysis buffer was collected for metformin quantification, while another 1 mL of phosphate-buffered saline (PBS) adjusted to the same pH was added into the system. The release solutions of metformin were measured at predetermined time points using the HPLC method for comparison. Using the same method as above, in vitro IR780 pH-triggered drug release from MI-PEOz-lip and MI-PEG-lip solutions were detected by UV–vis spectrometer.

Determination of ROS After SDT

1,3-diphenylisobenzofuran (DPBF) was also used as a probe to detect the production of ROS, as reaction with singlet-oxygen-generation could decrease the absorption intensity of DPBF centered at 410 nm. Briefly, 20 μL of DPBF was dissolved in 2 mL of DMSO (8 mM) and divided into free IR780 group, IR780-lip group, MI-PEOz-lip group and MI-PEOz-lip+pH 5.5 group (with the same IR780 concentration), then exposed to a portable US therapy device (Shengxiang Co., Shenzhen, China) with a 1 MHz transducer at 1 W/cm^2 and a continuous duty cycle. The absorption peak of DPBF at 410 nm was measured every 2 min by UV–vis spectrometer.

In vitro Cytotoxicity of MI-PEOz-Lip

The MDA-MB-231 human breast cancer cell line was obtained from the Cancer Epigenetics Laboratory (The Chinese University of Hong Kong, Hong Kong, China), which was originally purchased from American Type Culture Collection (ATCC, Manassas, VA, USA) and

cultured in high-glucose Dulbecco's modified Eagle medium (DMEM) supplemented with 10% fetal bovine serum (FBS) and 1% penicillin/streptomycin in a humidified atmosphere of 5% CO_2 at 37°C. To evaluate the cytotoxicity of MI-PEOz -lip, MDA-MB-231 cells were seeded into 96-well plates (1×10^4 cells/well) and incubated with different concentrations of MI-PEOz-lip for 24 h. Next, cell viability was tested by a typical CCK-8 assay. Then, the absorbance was recorded at 450 nm using a microplate reader (Bio Tek, ELX800, Winooski, VT, USA). To evaluate its in vitro therapeutic effect, MDA-MB-231 cells were incubated with IR780-PEOz-lip and MI-PEOz-lip for 18 h. These cells were cultured in an incubator containing an artificial hypoxic environment for 6 h and replaced with media at different pH values for 2 h. After 1 MHz ultrasonic irradiation (1 W/cm^2), the standard CCK8 assay was performed to measure cell viability.

Intracellular ROS production was studied by measuring the fluorescence intensity of dichlorofluorescein (DCF). DCFH-DA, a nonfluorescent cell permeant compound, is cleaved by endogenous esterases within the cell, and the de-esterified product can be converted into the fluorescent compound DCF upon oxidation by intracellular ROS. For quantitative analysis of intracellular ROS, MDA-MB-231 cells were incubated with DCFH-DA (10 μM) along with IR780-PEOz-lip and MI-PEOz-lip (containing 40 μg/mL IR780) in different pH media for 2 h under normoxic and hypoxic conditions. After 1 W/cm^2 US exposure for 1 min, the cells were washed twice with PBS. Finally, cells were observed under a confocal laser scanning microscope (CLSM, Nikon, Nikon-C2, Tokyo, Japan).

Measurement of the Oxygen Consumption Rate

We detected the oxygen consumption rate (OCR) of breast cancer cells treated with different nanoparticles combined with US to study the inhibitory effect of MI-PEOz-lip on cellular respiration by using MitoXpress Kit (Cayman Chemical, MI, USA). A 96-well plate was seeded with 1×10^4/well MDA-MB-321 cells and treated with free metformin, IR780-lip, MI-PEG-lip, MI-PEOz-lip and MI-PEOz-lip+pH 5.5 (each nanoparticle contains the same concentration of metformin and IR780). Subsequently, the cells of latter three groups were irradiated with 1 W/cm^2 US for 1 min. After 12 h treatment, each well was added with 10 μL of MitoXpress Xtra probe solution. The kinetic measurements were performed using a microplate reader, and a fluorescent signal was stably obtained (excitation 380 nm, emission 650 nm).

Measurement of Intracellular ATP Level

MDA-MB-231 cells were seeded on a 12-well plate at a concentration of 5×10^4 cells/well and cultured for 24 hours, and then incubated with free metformin, IR780-lip, MI-PEG-lip, MI-PEOz-lip and MI-PEOz-lip+pH 5.5 (each nanoparticle contains the same concentration of metformin and IR780) under sealed conditions and received US irradiation (1MHz, 1 min, 1 W/cm^2). The cells without any treatment under the sealed conditions were set as control group. The mediums were removed and the cells were collected. ATP assay kit (Abcam, Cambridge, UK) was employed following the manufacturer's instructions to measure the intracellular ATP level and the ATP values were recorded using a multi-functional microplate reader.

MDA-MB-231 Tumor-Bearing Mouse Model and in vivo Biodistribution

All animals were purchased from the Experimental Animal Center of Sun Yat-sen University. All experiments and procedures were conducted with the approval of the Institutional Animal Care and Use Committee of Sun Yat-sen University and according to the national guidelines on laboratory animal management. Female Balb/c nude mice were injected subcutaneously with MDA-MB-231 cells (2×10^6 cells in 50 μL per mouse).

To study the biodistribution of MI-PEOz-lip, female Balb/c nude mice carrying MDA-MB-231 tumors (n = 3) were injected intravenously with liposome solution (1 mg/kg). The in vivo IVIS imaging system (PerkinElmer, Massachusetts, USA) acquires fluorescence images at different time intervals. Major organs and tumors were harvested for ex vivo FI. The corresponding fluorescence intensities were analyzed by IVIS software.

In vitro and in vivo Photoacoustic Imaging

To evaluate the PAI performance of MI-PEOz-lip, a Vevo LAZR Photoacoustic Imaging System (VisualSonics Inc., Toronto, Canada) equipped with an LZ250 probe was used to acquire PAI and US images. MI-PEOz-lip solution at a concentration of 0.5 mg/mL was scanned for PAI at different wavelengths ranging from 680 nm to 970 nm (interval = 5 nm) to detect the maximum absorbance for the optimized PAI. The quantified PAI signal intensity

within the region of interest (ROI) of each image was then analyzed by Vevo LAZR software.

For the in vivo PAI, MDA-MB-231 tumor-bearing mice with a volume of approximately 100 mm^3 were intravenously injected with 200 μL of MI-PEOz-lip (1 mg/kg IR780). PAI images were then taken at different time points, and the average PAI intensity in the tumor area was measured.

In vivo Sonodynamic Therapy

MDA-MB-231 tumor-bearing mice were randomly divided into five groups (n = 5 in each group) and intravenously injected with PBS, IR780-lip, MI-PEG-lip, and MI-PEOz-lip (dose of IR780 = 2 mg/kg, dose of metformin = 10 mg/kg). In the US treatment groups, tumors were treated with 2.5 W/cm^2 US for 5 min at 12 h after injection, and the treatment effects at each time point were compared. After treatment, tumor size and body weight were monitored every 2 days for 15 days, and tumor volume was calculated according to the following formula: $width^2 \times length/2$.

Histological Examination and Immunofluorescence Analysis

To further detect the effect of in vivo treatment, hematoxylin-eosin (H&E) staining and terminal deoxynucleotidyl transferase-mediated dUTP-biotin nick end labeling (TUNEL) assays were used to stain the tumor sections. After 15 days of US exposure, tumor tissues from the different groups were harvested, fixed in 10% neutral-buffered formalin, embedded in paraffin, and sectioned at 8 μm thickness. After H&E staining, the tumor sections were examined using a digital microscope. The heart, liver, spleen, lung and kidney were collected at the same time, and biosafety analysis was performed by H&E staining. For the TUNEL assay, the tumor sections were stained using an In Situ Cell Death Detection Kit and visualized by CLSM.

Pimonidazole hydrochloride (MKBio, Hypoxyprobe™, Shanghai, China) was utilized to assess tumor hypoxia levels. Mice with MDA-MB-231 tumors with a volume of approximately 100 mm^3 were injected intravenously with free metformin, MI-PEG-lip and MI-PEOz-lip. After 24 h, the mice were injected intraperitoneally with pimonidazole hydrochloride (0.6 mg per mouse). The mice were then sacrificed to collect the tumor tissues after 90 min. The tumors were then embedded in optimal cutting temperature (OCT) compound and cut into 8 μm sections for further staining. To detect pimonidazole, which binds to thiol-containing biomolecules/tissues in an oxygen-deficient environment, mouse anti-pimonidazole monoclonal antibody (dilution 1:100) was used as the primary antibody, with Alexa Fluor 488-conjugated goat anti-mouse secondary antibody (dilution 1:200). Finally, stained sections were analyzed by CLSM.

Statistical Analysis

Mean ± SD values were used for the expression of data unless otherwise specified. Statistical analyses of data were performed using Student's *t*-test. Differences of *P < 0.05 and **P < 0.01 were considered statistically significant.

Results and Discussion

Characterization of MI-PEOz-Lip

Liposomes have been widely used as drug delivery systems due to their versatile loading capacity for both hydrophilic and hydrophobic drugs. Therefore, pH-responsive liposomes were chosen as the drug loading nanoplatform for metformin and IR780 in this study. Metformin molecules are highly water soluble and could be encapsulated within the hydrophilic cavity of liposomes. Instead, IR780 was loaded into the hydrophobic liposomal lipid bilayer. The resulting MI-PEOz-lip was prepared according to a standard protocol (see the Materials and methods for details). MI-PEOz-lip could efficiently accumulate in the tumor region during blood circulation through the typical EPR effect. After entering the tumor site, the pH-sensitive liposome delivery system could take advantage of the reduced pH of the tumor tissue to undergo structural changes and release the encapsulated metformin in a spatially controlled manner, thereby reducing oxygen consumption and enhancing IR780-induced SDT (Figure 1).

TEM images of MI-PEOz-lip exhibited a typical phospholipid bilayer structure and a uniform size distribution (Figure 2A). The average hydrodynamic diameters of MI-PEOz-lip and MI-PEG-lip were 220.193 nm and 190.137 nm, the zeta potentials were −33.69 mV and −23.88 mV, and particle dispersion indices were 0.165 and 0.189, respectively, as measured by the typical dynamic light scattering method (Figure 2BC). This demonstrated that the pH-responsive phospholipids could have the same morphology and structure as the common PEG-modified liposomes. MI-PEOz-lip also showed satisfactory stability when incubated

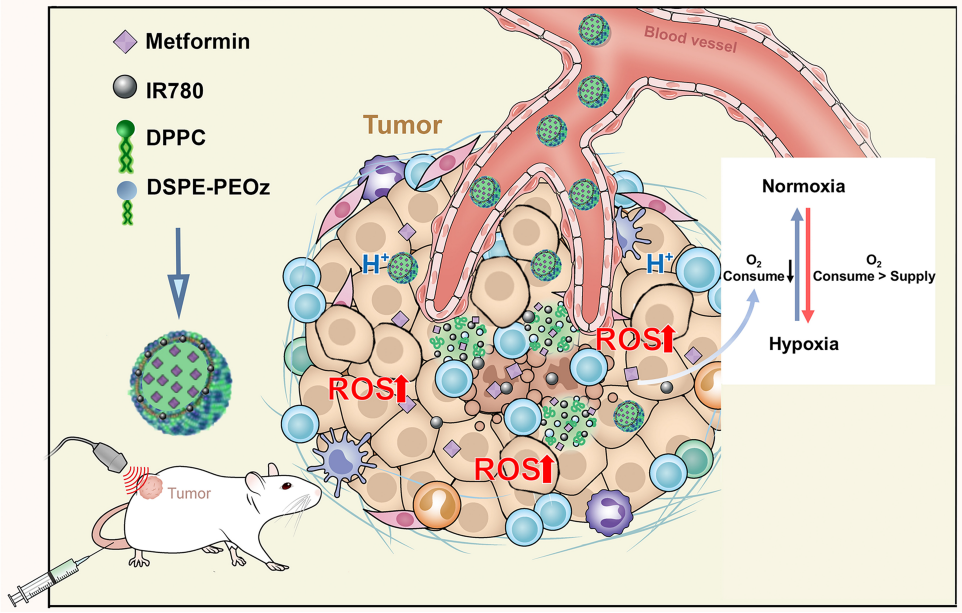

Figure 1 Schematic illustration of self-synthesized MI-PEOz-lip and its proposed antitumor mechanism. After intravenous injection, MI-PEOz-lip is expected to accumulate in tumors via the EPR effect. Then, the incorporation of pH-sensitive lipids into this liposome allows metformin to be rapidly released at the tumor site in response to the acidic pH of the tumor microenvironment. The released metformin reverses hypoxia in the tumor by reducing oxygen consumption and further increases IR780 to produce more ROS in hypoxic tumors.

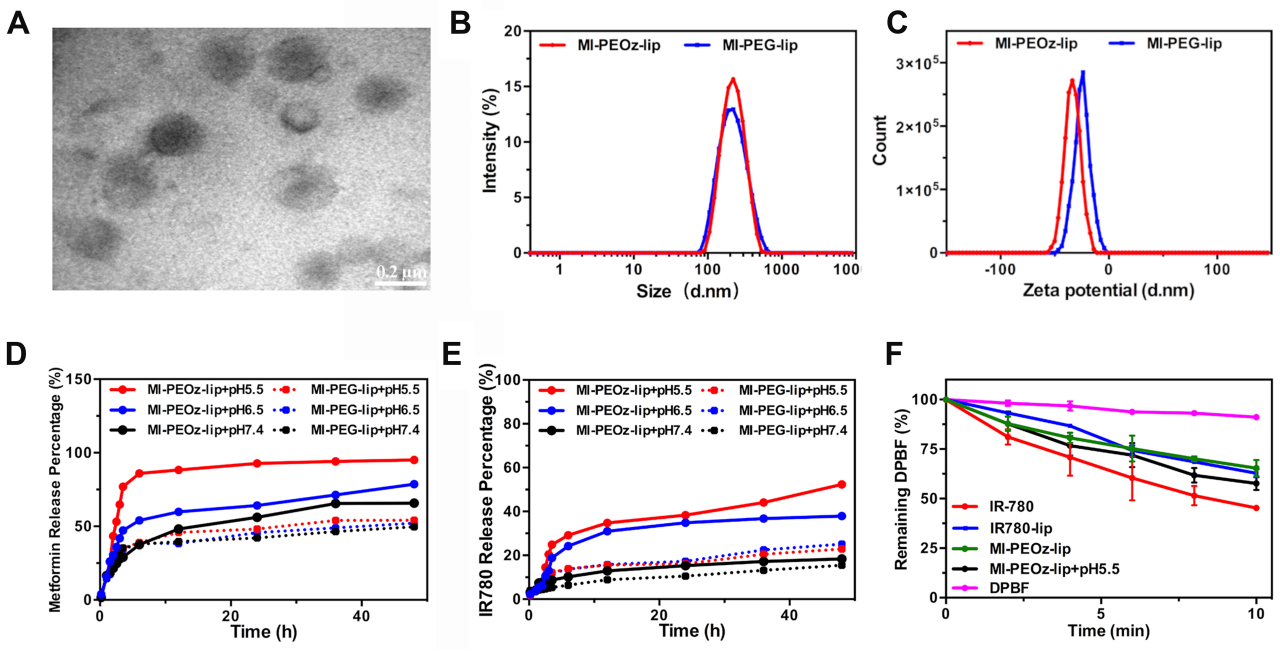

Figure 2 Characterization of the MI-PEOz-lip. (**A**) The morphology of MI-PEOz-lip. Scale bar: 200 nm. (**B**–**C**) The size distribution and zeta potentials of MI-PEOz-lip and MI-PEG-lip were measured by the dynamic light scattering technique. (**D**–**E**) Metformin and IR780 release characteristics of MI-PEOz-lip and MI-PEG-lip in PBS at pH 5.5, 6.5 and 7.4 during 48 h of incubation. (**F**) Changes in the absorption intensity of DPBF after US incubation with different reagents.

in PBS at 4°C, with no obvious change observed in its hydrodynamic diameter or surface charge after 7 days (Figure S1). To further investigate the influence of pH, the morphological structure of MI-PEOz-lip after the reaction at pH 5.5 was detected (Figure S2), showing that the phospholipid bilayer structure of MI-PEOz-lip became incomplete.

Moreover, the size of MI-PEOz-lip became much smaller at pH 5.5 than that kept at pH 7.4,[32,33] likely reflecting the disassembly process of PEOzylated liposome triggered by the acidic environment. The zeta potential of MI-PEG-lip almost did not change when pH decreased; by contrast, the zeta potential of MI-PEOz-lip reduced significantly (Figure S3). Thus, it suggested that MI-PEOz-lip could change in structure to release cargo in the acidic environment. The absorbance spectrum of the MI-PEOz-lip showed a characteristic metformin absorption peak at 232 nm, along with characteristic IR780 peaks at 783 nm, thus confirming the successful encapsulation efficiency of both reagents (Figure S4). The encapsulation efficiency of metformin and IR780 was measured using HPLC and UV-Vis-spectrophotometry. Metformin and IR780 showed a concentration-dependent increase in absorbance intensity and were described by the following linear correlation equations: $Y = 89155X - 57954$ ($R^2 = 0.9987$) and $Y = 0.017X + 0.0137$ ($R^2 = 0.9985$) (Figure S5). According to the calibration curve of metformin and IR780, the loading efficiencies of metformin and IR780 were calculated to be approximately 18% and 84%, respectively.

To evaluate the release behavior of MI-PEOz-lip, we detected the release of metformin and IR780 by MI-PEOz-lip and MI-PEG-lip at different pH values. The results of drug release tests indicated that the metformin release rate of MI-PEOz-lip was 49.7% after 48 h incubation at pH 7.4 PBS. The accumulative release amount of metformin by MI-PEOz-lip increased to 64.13% at pH 6.5, while at pH 5.5, almost 95% of the loaded drug was released within 24 h. The cumulative release of metformin at acidic pH was higher than that at pH 7.4, while MI-PEG-lip did not release significantly under acidic conditions (Figure 2D). Furthermore, we investigated the drug release behaviors of IR780 from MI-PEOz-lip and MI-PEG-lip at different pH values (Figure 2E). Merely 18.39% of IR780 from MI-PEOz-lip was released at pH 7.4 after 48 h. At pH 6.5 and 5.5, IR780 from MI-PEOz-lip release was slightly accelerated, while MI-PEG-lip did not exhibit efficient drug release under acidic conditions. These results indicate that the incorporation of the sensitive lipid DSPE-PEOz successfully enabled MI-PEOz-lip to release its cargo depending on pH, which facilitated the release of metformin and IR780 in the weakly acidic tumor microenvironment and especially in the lysosomal compartment in tumor cells (pH 5.0–6.2).[34] PEOz is synthesized by cationic ring-opening polymerization and has good hydrophilicity, biocompatibility, low toxicity and no immunogenicity. In recent years,[35] PEOz has exhibited broad application prospects in drug delivery systems because its pH sensitivity is very beneficial for achieving the rapid release of drugs in acidic conditions, such as in tumor tissue and the endosome-lysosome system. The "N" in the amide bond of the PEOz chain and its corresponding resonance structure easily combine with hydrogen ions in the solution system and form hydrogen bonds with other amide groups in or between the molecules of PEOz. Under acidic conditions, the formation of a large number of hydrogen bonds will destroy PEOz to form liposomes. The core-shell structure reduces the stability of liposomes and quickly releases the encapsulated drug. Therefore, with effective sensitivity to pH, this liposome can intelligently release metformin and IR780 at the tumor site with a therapeutic window concentration to reduce the OCR and has great potential for amplifying the efficacy of SDT.

To further investigate the ROS generating capability of MI-PEOz-lip in vitro, a typical ROS analysis probe, DPBF, was applied to detect the production of ROS because it could be oxidized by ROS generation, triggering a decline in the peak of characteristic absorbance intensity at 410 nm. With increasing US processing time, the DPBF absorbance intensity significantly decreased with MI-PEOz-lip and IR780-lip after US exposure at 1 W/cm^2 for 10 min, indicating that MI-PEOz-lip and IR780-lip could generate a large amount of ROS content in IR780 after US irradiation. The ROS produced by MI-PEOz-lip and IR780-lip have the same efficiency (Figure 2F), indicating that the loading of metformin does not affect the sonodynamic characteristics of IR780. Moreover, the DPBF absorbance of MI-PEOz-lip gradually decreased under the acidic environment, which also demonstrated the pH-responsive release of IR780 could further enhance the generation of ROS. However, the ROS generated from both liposomal IR780 formulations appeared to be slightly less efficient than that of free IR780, which likely reflects the extent of IR780 self-quenching at high density in liposomes.

In vitro Cytotoxicity and Antitumor Efficacy of MI-PEOz-Lip

Next, the therapeutic ability of SDT mediated by MI-PEOz-lip to treat MDA-MB-231 breast cancer cells in vitro was investigated. First, the cytotoxicity of this liposome was measured, and the cytotoxicity of MI-PEOz-lip to breast cancer cells was observed under different reagent concentrations. No significant cytotoxicity of MI-PEOz-lip was

observed after incubating breast cancer cells for 24 h in dark conditions, indicating the excellent biocompatibility of MI-PEOz-lip (Figure 3A). To further demonstrate that MI-PEOz-lip could reduce oxygen consumption during hypoxia in response to pH to improve SDT, we evaluated the in vitro cytotoxicity of sonodynamic effects. US alone had less effect on cells under normoxic and hypoxic conditions. IR780-PEOz-lip and MI-PEOz-lip had no obvious changes in tumor cell damage without US irradiation, which indicates that the generation of ROS in the area of US radiation can locally kill tumor cells and reduce damage to surrounding normal tissues. Notably, IR780-PEOz-lip and MI-PEOz-lip showed no significant difference in tumor cell damage from US irradiation under normoxic conditions, because normoxia can enhance the SDT effect of both IR780-loaded nanoplatform. Under hypoxic conditions, MI-PEOz-lip was significantly more cytotoxic than IR780-PEOz-lip, especially in acidic environment. These results demonstrated that metformin in MI-PEOz-lip could respond to acidic release while acting synergistically (Figure 3B).

According to reports, metformin can inhibit the mitochondrial respiratory chain of cancer cells, thereby reducing inherent oxygen consumption to overcome tumor hypoxia. To investigate the inhibitory effect of MI-PEOz-lip on cell respiration, the OCRs of MDA-MB-231 cells treated with different formulations were examined using the MitoXpress Kit. As shown in Figure 3C, MI-PEOz-lip showed similar inhibitory effects on cell respiration as the free drugs. Notably, MI-PEOz-lip had better efficacy under acidic conditions than other nanoparticles, and its OCR was reduced by approximately 74%, demonstrating that MI-PEOz-lip could rapidly release metformin and better inhibit cell respiration under acidic conditions. To assess the impact of metformin on inhibiting mitochondrial respiratory chain, the ATP levels in MDA-MB-231 cells were evaluated. As shown in Figure 3D, compared with the IR780-lip group, the ATP content generated by MDA-MB-231 cells was significantly reduced in the MI-PEOz-lip group, especially under acidic conditions, indicating that the addition of metformin ensured the inhibition of mitochondrial respiration function, thereby reducing ATP generation in MDA-MB-231 cells.

To verify the in vitro ability of intracellular MI-PEOz-lip to generate ROS by US, the common ROS indicator 2′,7′-dichlorofluorescein diacetate (DCFH-DA) was used.

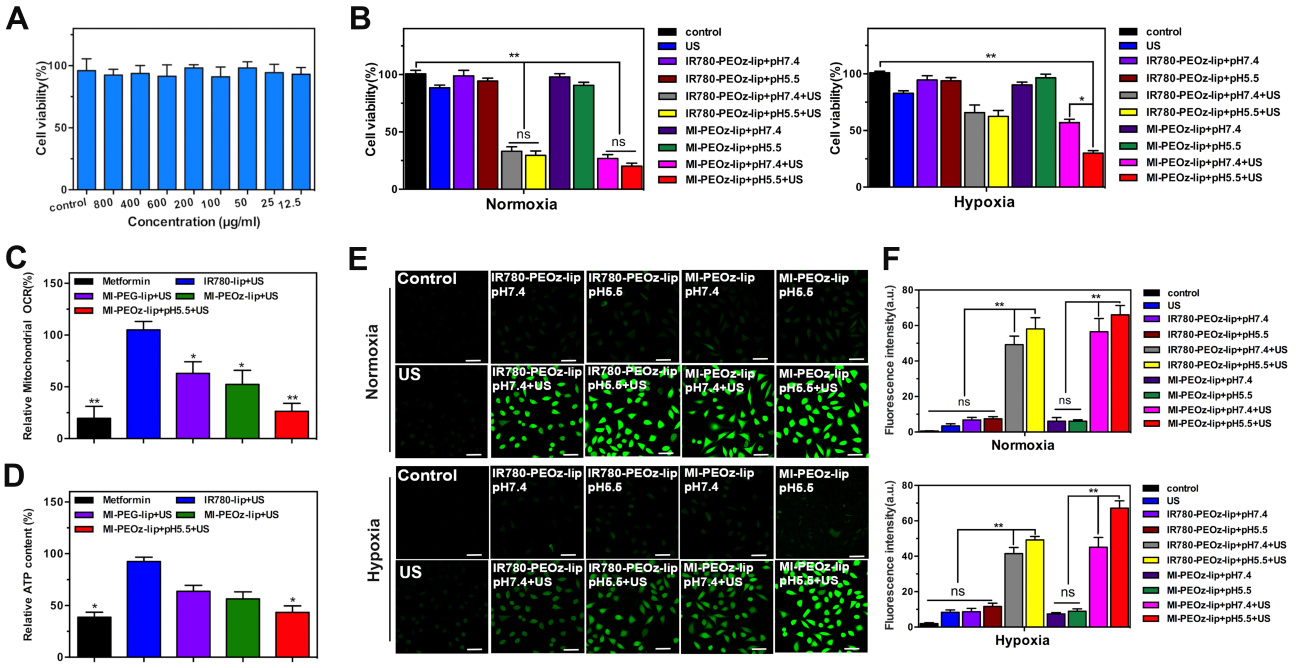

Figure 3 Cytotoxicity of MI-PEOz-lip and in vitro sonodynamic treatment of cancer cells. (**A**) After 24 h of incubation with MDA-MB-231 cells, the cytotoxicity of MI-PEOz-lip was detected by CCK8. (**B**) Cell viabilities of MDA-MB-231 cells were measured by CCK8 after incubation with MI-PEOz-lip (80 μg/mL) followed by US irradiation at different pH values under normoxic and hypoxic conditions (*p <0.05, **p <0.01). (**C**) The relative OCR of MDA-MB-231 cells were detected after different treatments under the sealed condition (*p <0.05, **p <0.01). (**D**) Mitochondrial respiratory depression was evaluated through the relative ATP content of MDA-MB-231 cells received indicated treatments under the sealed condition. (**E**–**F**) CLSM images of ROS formation in MDA-MB-231 cells with different treatments with and without DCFH-DA staining (green) to evaluate intracellular ROS generation (**p <0.01). The corresponding quantitative analysis of ROS fluorescence intensity. (n = 3, mean ± SD, scale bar 50 μm).

Weak green fluorescence appeared after MI-PEOz-lip and IR780-PEOz-lip incubation in the absence of US under normoxic and hypoxic conditions due to the photosensitive effect of IR780. In contrast, the cells treated with US alone exhibited no green fluorescence. As expected, the breast cancer cells incubated with MI-PEOz-lip and IR780-PEOz-lip under acidic or neutral pH medium exhibited the same strong green fluorescence under normoxic conditions after US irradiation. Importantly, under hypoxic conditions, the green fluorescence was strong in MDA-MB-231 cells incubated with MI-PEOz-lip, while the cells incubated with IR780-PEOz-lip showed weak green fluorescence after US irradiation (Figure 3EF), implying that the saved oxygen boosted the generation of ROS. Moreover, the fluorescence intensity in MI-PEOz-lip group under acidic environment was much stronger, indicating that MI-PEOz-lip exhibited local site-specific release ability to improve drug bioavailability and reduce tumor cell oxygen consumption, which is triggered by US to generate ROS to enhance antitumor efficiency.

In vivo Biodistribution

The in vivo behavior of MI-PEOz-lip was then investigated by utilizing the intrinsic fluorescence of IR780 to track the in vivo delivery and biodistribution. Mice bearing MDA-MB-231 breast cancer tumors were intravenously injected with MI-PEOz-lip, and fluorescence images were acquired at various time points. As shown in Figure 4A, MI-PEOz-lip gradually accumulated in the tumor area over time via the EPR effect, as indicated by increasing IR780 fluorescence within tumors. The value of the fluorescence signal at the tumor site was significantly increased at 12 h after MI-PEOz-lip injection. The high tumor uptake of these liposomes was confirmed with ex vivo fluorescence images of the major organs (liver, spleen, kidney, heart, lung) and tumors at 12 h postinjection, and then we measured the average IR780 fluorescence intensity of these organs and tumors (Figure 4BC). The tumor showed the highest fluorescent intensity compared with the organs, including the heart, liver, spleen, lung and kidneys, indicating that these MI-PEOz-lips accumulated effectively in tumor tissue.

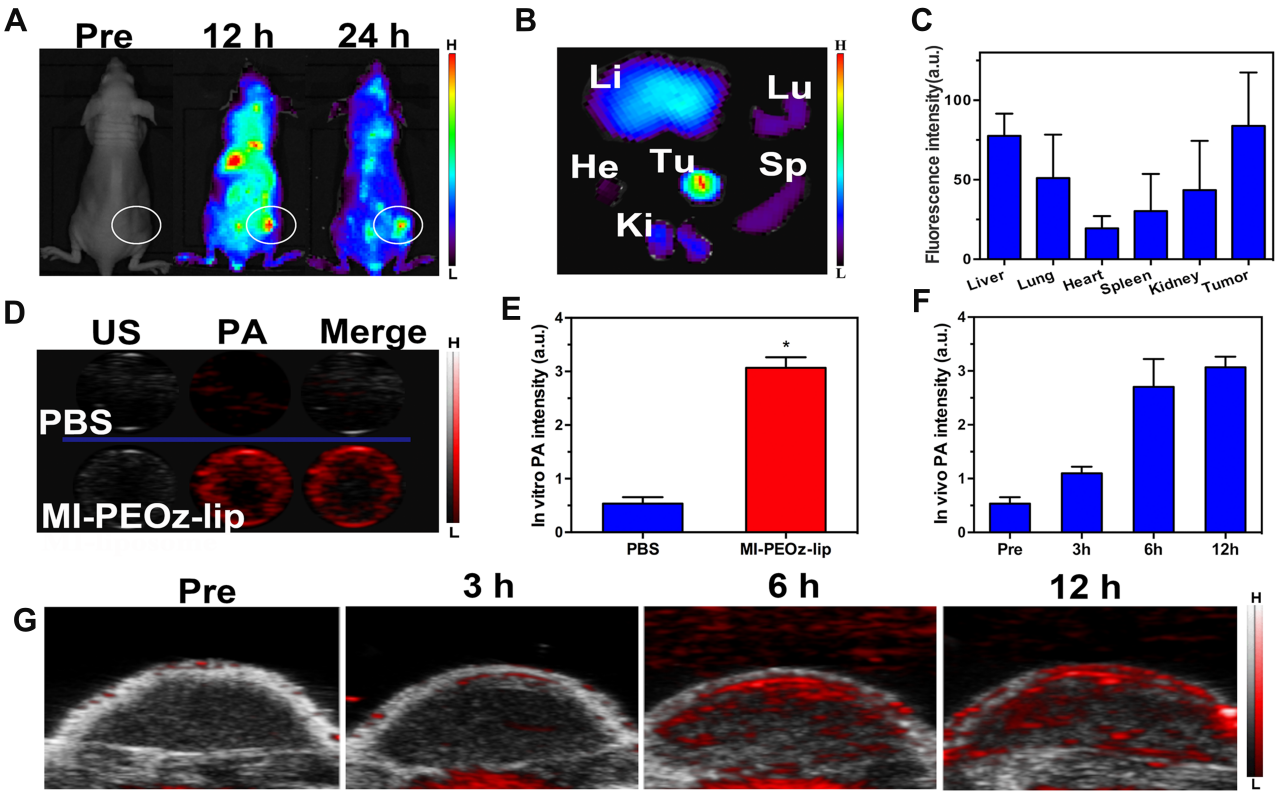

Figure 4 In vivo biodistribution and PA imaging assessment of MI-PEOz-lip. (**A**) NIR FI of tumor-bearing mice after the intravenous administration of MI-PEOz-lip at different time points (pre, 12 h, 24 h). White circles indicate the location of MDA-MB-231 tumors. (**B**) Ex vivo FI of the main organs and tumors of mice 12 h after injection. (**C**) Corresponding fluorescence signal intensity. The values are expressed as the mean ± SD, n=3 per group. (**D**) In vitro PA imaging of MI-PEOz-lip at a concentration of 0.5 mg/mL compared to PBS. (**E**) Quantitative PA signal intensity of MI-PEOz-lip and PBS (n = 3, mean ± SD, *p<0.05). (**F**) Corresponding quantitative analysis of enhanced PA signal intensity (n = 3, mean ± SD) and (**G**) PA imaging of tumors before and after intravenous MI-PEOz-lip (3 h, 6 h, and 12 h).

However, the fluorescence intensity of the liver tissue also remained. This is because the nanoparticles also accumulated in the liver, for the following reasons. IR780 is metabolized by the liver,[36] and liver Kupffer cells play a role in its uptake and degradation by phagocytosis. However, in the case of SDT, this may not be a critical issue because the tumor area can be treated locally to reduce damage to surrounding normal tissues. The above results suggested that MI-PEOz-lip effectively accumulates in tumor tissues for subsequent effective cancer diagnosis and treatment.

In vitro and in vivo Photoacoustic Imaging

PAI is an optical imaging technique that uses the thermoelastic expansion of tissues under irradiation to generate US waves detected by a transducer. The thermoelastic expansion of the tissue depends on the absorption of light at the excitation wavelength. Inspired by the ideal light absorption in the near infrared region reflected by the excellent contrast agent for PAI, MI-PEOz-lip was further evaluated to determine its diagnostic imaging performance for PAI. B-mode US images, PAI images, and overlay images (B-mode and PAI-mode) of MI-PEOz-lip are shown in Figure 4DE. MI-PEOz-lip showed contrast enhancement in PAI imaging because of the strong absorption in the NIR range, but no contrast change was observed in PBS, indicating that the encapsulated IR780 contributed to the PAI signal enhancement.

The in vivo PAI performance of MI-PEOz-lip was further evaluated in tumor-bearing mice. After intravenous injection of MI-PEOz-lip, the PAI signal in vivo gradually increased with observation time, indicating that MI-PEOz-lip gradually accumulated in the tumor area. The PAI signal enhancement was further quantitatively analyzed by the PAI signal intensity in the ROI. PAI signaling at the tumor site was detected as early as 3 h after injection. At 6 h after injection, a strong PA signal was observed in the tumor and was significantly different from that in surrounding normal tissue. In addition, the in vivo tumor PA signal increased significantly and continuously over time. The PAI intensity of the tumor at 12 h was approximately 6 times higher than that before injection (Figure 4FG). Notably, PA imaging is easy to obtain from traditional ultrasonic images due to its integration with ultrasonic transducers. Overlaying PA images and US images can provide morphological information and reveal the distribution of contrast agents in tumor tissues. The results indicated that MI-PEOz-lip can be used as a good PAI contrast agent for tumor diagnostic imaging.

In vivo Alleviation of Hypoxia and Increased Antitumor Efficacy

After confirming the accumulation and retention of the MI-PEOz-lip in tumors, we performed in vivo experiments using the MDA-MB-231 tumor model to evaluate the efficacy of this liposome-mediated SDT treatment. MDA-MB-231 tumor-bearing mice (approximately 100 mm^3 in size) were randomly divided into five groups (n = 5), namely, PBS, MI-PEOz-lip, IR780-lip + US, MI-PEG-lip + US and MI-PEOz-lip + US (n = 5), and the drugs were injected intravenously. In the last three groups, the tumor areas were irradiated and exposed to 1 MHz US at 2.5 W/cm^2 for 5 min at 12 h after injection.

Following treatment, the tumor volume of mice in each group was measured using a digital caliper every two days. The change in absolute tumor size over time is shown in Figure 5A. Compared with the PBS group, the MI-PEOz-lip group and the IR780-lip + US group showed only a slight inhibitory effect. However, in obvious contrast with these three groups, tumor growth in the MI-PEG-lip and MI-PEOz-lip groups was significantly suppressed after 5 minutes of US irradiation. It is worth noting that tumor growth was significantly delayed after treatment due to the rapid drug release of MI-PEOz-lip in response to the acidic microenvironment of tumors, while tumors in other treatment groups were still significantly present (Figure 5B). Decreased pH induces PEOz to undergo a conformational change and adsorb tightly on the surface of the liposomal membrane. The lipid bilayer of the liposomes rearranges to accommodate the adsorptive PEOz chain. Upon damage in the liposome bilayer or fusion between membranes, the drug is quickly released. These results indicate that pH-triggered drug release contributed to the enhanced therapeutic efficacy of MI-PEOz-lip. The negligible change in relative body weight until the end of treatment indicated the safety of this liposome (Figure 5C).

We further investigated the therapeutic efficacy of the different treatment groups by H&E staining. The TUNEL assay was also used to study the morphological changes and tumor cell apoptosis. Mice from the different treatment groups were sacrificed. H&E staining revealed more necrotic regions in the MI-PEOz-lip-mediated SDT group, while moderate damage was found in tumors in the MI-PEG-lip-mediated SDT group. Damage was also found in the IR780-lip-mediated SDT group, while no significant damage was seen in the other two groups. Similar results were obtained with the TUNEL assay, and the cells emitted bright green fluorescent signals in tumors treated with the MI-PEOz-lip under US exposure, indicating that the maximum amount of cell

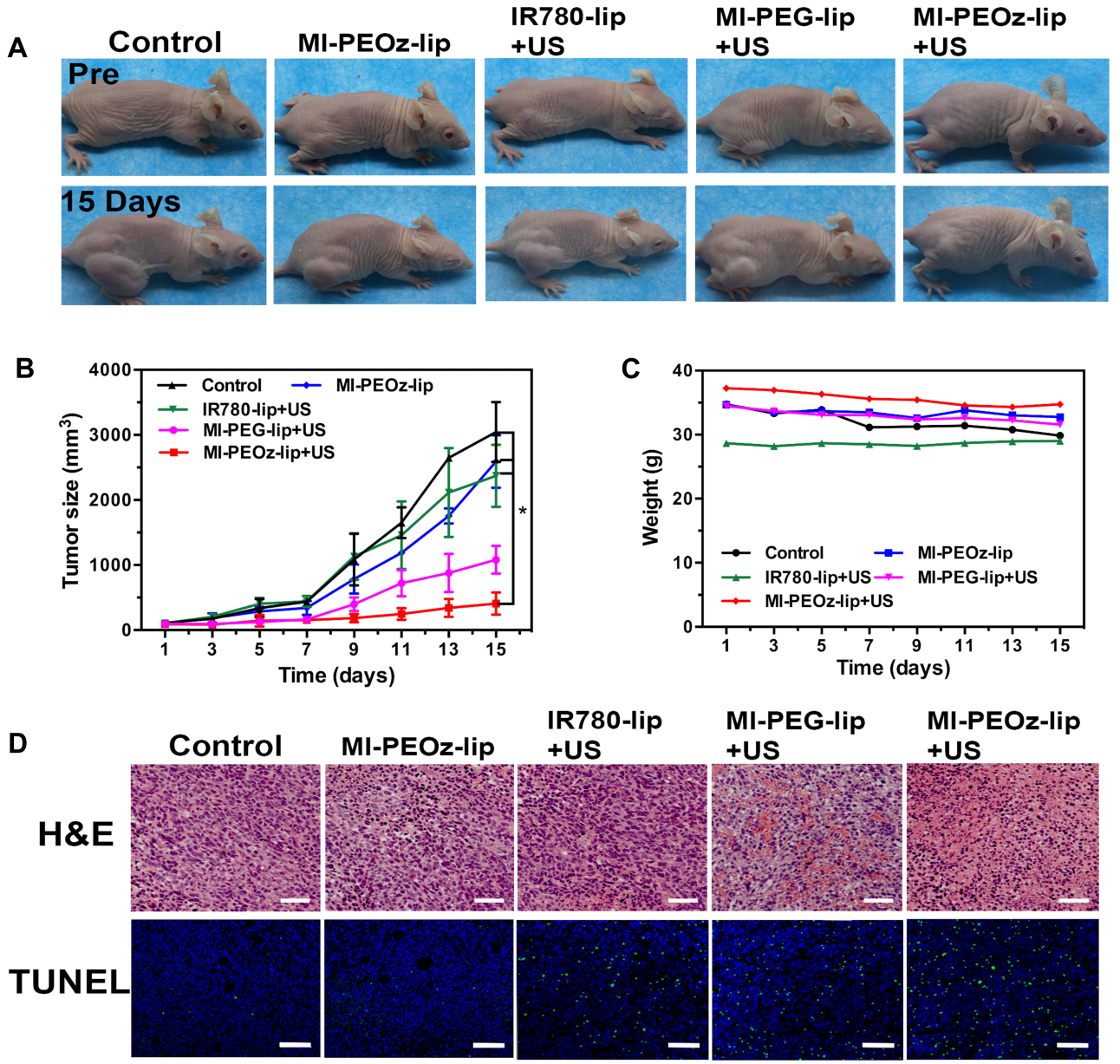

Figure 5 In vivo SDT efficiency of MI-PEOz-lip. (**A**) Photographs of MDA-MB-231 tumor-bearing mice before and 15 days after MI-PEOz-lip-assisted SDT treatment. (**B**) Tumor growth curves of the five groups after receiving various treatments (n = 5, mean ± SD, *P <0.05). (**C**) Weight curves of the five groups after different treatments (n = 5, mean ± SD). (**D**) H&E staining and TUNEL staining of tumor sections after various treatments. The scale bars are 50 μm and 100 μm.

apoptosis occurred in the MI-PEOz-lip group compared with the other groups (Figure 5D). To further clarify the above-mentioned mechanism of SDT enhancement in vivo, an ex vivo immunofluorescence staining experiment was performed to verify the oxygen content in the tumor. Tumor-bearing mice were sacrificed, and tumor tissues were collected, sectioned, and stained with Hypoxyprobe-1 and DAPI fluorescein stain 24 h after injection of drugs. The area where the drug was distributed showed significant elimination of hypoxia. In addition, compared with the control PBS, free metformin, and MI-PEG-lip, MI-PEOz-lip significantly reduced the distribution of hypoxia in tumors, as illustrated by quantitative hypoxia fluorescence. Importantly, the tumors all exhibited a significant improvement in oxygenation when MI-PEOz-lip was injected compared to MI-PEG-lip (Figure 6AB). These results indicate that pH-responsive liposomes can release large quantities of metformin in tumors, thereby greatly improving tumor oxygenation in various model systems. Overall, the results of immunofluorescence staining indicate that MI-PEOz-lip can better relieve hypoxia in tumor tissue and further improve SDT.

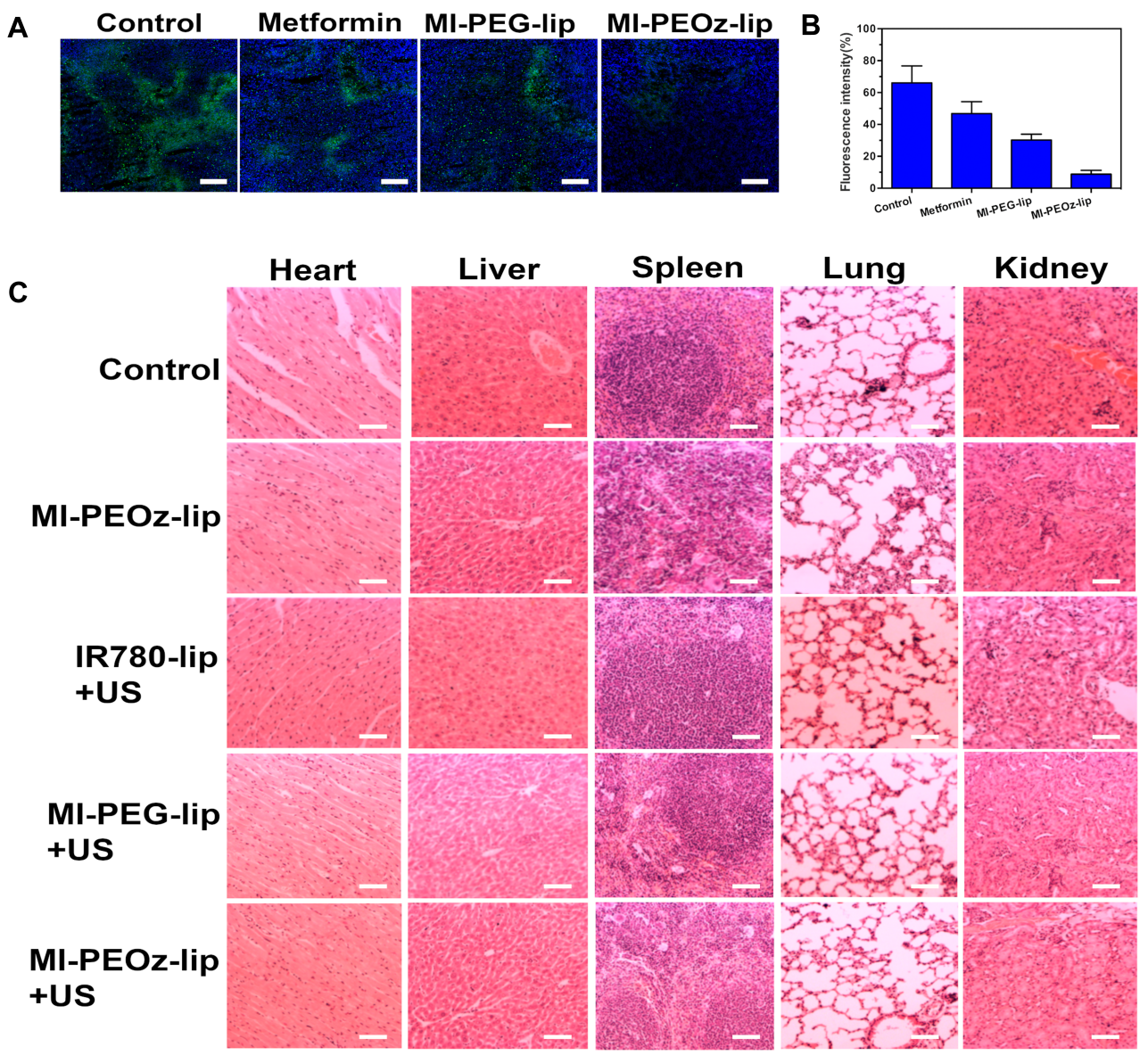

Figure 6 Enhanced oxygenation effect of MI-PEOz-lip and H&E staining of major organs. (**A**) Representative immunofluorescence images of MDA-MB-231 tumor sections stained with Hypoxyprobe™. Scale bar: 200 μm. (**B**) Quantification of tumor hypoxia from the images shown in (**A**). (**C**) H&E staining of the major organs (heart, liver, spleen, lung, and kidney) of MDA-MB-231 tumor-bearing nude mice after various treatments. Scale bar: 50 μm.

Reducing the oxygen consumption of cells to improve hypoxia will indirectly increase the oxygen content of tumor tissues, which directly influences the effectiveness of SDT because fatal ROS are generated from oxygen. Taken together, these results demonstrate the exciting potential of MI-PEOz-lip-mediated SDT as a treatment that could not only efficiently deliver the sonosensitizer IR780 to tumors but also effectively reverse tumor hypoxia, thereby enhancing the therapeutic effect of SDT. In addition, the in vivo toxicity of MI-PEOz-lip-mediated SDT was evaluated in major organs (heart, liver, spleen, lung, and kidney) by H&E staining. No significant histopathological changes were found in the main organs after the 15th day of treatment. Negligible body weight fluctuations and H&E staining of major organs demonstrated that MI-PEOz-lip-mediated SDT had few adverse effects on mouse health and normal organs (Figure 6C). The results indicate that these liposomes are biocompatible, and they are therefore expected to become potential clinical drugs. Moreover, since hypoxia is effectively reduced, this strategy can be applied to other therapies that use oxygen as a key component, such as radiotherapy, which is widely used as a first-line treatment for many types of cancer.

Conclusion

In summary, we have developed pH-responsive liposomes based on the sonosensitizer IR780 and the antihyperglycemic drug metformin to reduce oxygen consumption for highly effective tumor SDT, and the effects been systematically validated in vitro and in vivo. In vivo and ex vivo FI showed that MI-PEOz-lip had a long blood circulation half-life and a high tumor absorption rate in vivo because of the EPR effect. The pH-responsive liposomes released the drug in the tumor at a specific site, reaching the therapeutic window concentration and thereby reducing the oxygen consumption in the tumor area. MI-PEOz-lip has great potential to improve tumor oxygenation and increase IR780 transmission, which can contribute to significantly enhancing the efficacy of SDT in vivo, thus opening up a new approach to constructing therapeutic drugs with high biosafety and ideal therapeutic properties.

Acknowledgments

The authors are grateful to Dr. Qinqin Jiang and Weiwei Liu for assistance with the PAI. This work was financially supported by the National Natural Science Foundation of the People's Republic of China (Grant No. 81530055) and the China Postdoctoral Science Foundation (Grant No. 2019M653202, 2019M653200).

Disclosure

The authors report no conflicts of interest in this work.

References

1. Meng Z, Zhou X, Xu J, et al. Light-triggered in situ gelation to enable robust photodynamic-immunotherapy by repeated stimulations. *Adv Mater*. 2019;31(24):e1900927. doi:10.1002/adma.201900927
2. Song W, Kuang J, Li CX, et al. Enhanced immunotherapy based on photodynamic therapy for both primary and lung metastasis tumor eradication. *ACS Nano*. 2018;12(2):1978–1989. doi:10.1021/acsnano.7b09112
3. Hu D, Sheng Z, Gao G, et al. Activatable albumin-photosensitizer nanoassemblies for triple-modal imaging and thermal-modulated photodynamic therapy of cancer. *Biomaterials*. 2016;93:10–19. doi:10.1016/j.biomaterials.2016.03.037
4. Agostinis P, Berg K, Cengel KA, et al. Photodynamic therapy of cancer: an update. *CA Cancer J Clin*. 2011;61(4):250–281. doi:10.3322/caac.20114
5. Qian X, Zheng Y, Chen Y. Micro/nanoparticle-augmented sonodynamic therapy (SDT): breaking the depth shallow of photoactivation. *Adv Mater*. 2016;28(37):8097–8129. doi:10.1002/adma.201602012
6. al-Watban FA. Photodynamic therapy: tumor volume limitation and tumor response for murine fibrosarcoma. *Lasers Surg Med*. 1990;10(2):165–172. doi:10.1002/lsm.1900100209
7. Altan L, Kasapoğlu Aksoy M, Kösegil Öztürk E. Efficacy of diclofenac & thiocolchioside gel phonophoresis comparison with ultrasound therapy on acute low back pain; a prospective, double-blind, randomized clinical study. *Ultrasonics*. 2019;91:201–205. doi:10.1016/j.ultras.2018.08.008
8. Luo Z, Jin K, Pang Q, et al. On-demand drug release from dual-targeting small nanoparticles triggered by high-intensity focused ultrasound enhanced glioblastoma-targeting therapy. *ACS Appl Mater Interfaces*. 2017;9(37):31612–31625. doi:10.1021/acsami.7b10866
9. Trédan O, Galmarini CM, Patel K, Tannock IF. Drug resistance and the solid tumor microenvironment. *J Natl Cancer Inst*. 2007;99(19):1441–1454. doi:10.1093/jnci/djm135
10. Harada H. How can we overcome tumor hypoxia in radiation therapy? *J Radiat Res*. 2011;52(5):545–556. doi:10.1269/jrr.11056
11. Wang B, Zhai Y, Shi J, et al. Simultaneously overcome tumor vascular endothelium and extracellular matrix barriers via a non-destructive size-controlled nanomedicine. *J Controlled Release*. 2017;268:225–236. doi:10.1016/j.jconrel.2017.10.029
12. Duong HTT, Kamarudin ZM, Erlich RB, et al. Intracellular nitric oxide delivery from stable NO-polymeric nanoparticle carriers. *Chem Commun*. 2013;49(39):4190–4192. doi:10.1039/C2CC37181B
13. Tang X, Cheng Y, Huang S, et al. Overcome the limitation of hypoxia against photodynamic therapy to treat cancer cells by using perfluorocarbon nanodroplet for photosensitizer delivery. *Biochem Biophys Res Commun*. 2017;487(3):483–487. doi:10.1016/j.bbrc.2017.03.142
14. Cheng Y, Cheng H, Jiang C, et al. Perfluorocarbon nanoparticles enhance reactive oxygen levels and tumour growth inhibition in photodynamic therapy. *Nat Commun*. 2015;6:1. doi:10.1038/ncomms9785
15. Huang W-C, Shen M-Y, Chen -H-H, et al. Monocytic delivery of therapeutic oxygen bubbles for dual-modality treatment of tumor hypoxia. *J Control Release*. 2015;220(Pt B):738–750. doi:10.1016/j.jconrel.2015.09.016
16. Simon-Yarza T, Mielcarek A, Couvreur P, Serre C. Nanoparticles of metal-organic frameworks: on the road to in vivo efficacy in biomedicine. *Adv Mater*. 2018;30(37):1707365. doi:10.1002/adma.201707365
17. Lu G, Li S, Guo Z, et al. Imparting functionality to a metal–organic framework material by controlled nanoparticle encapsulation. *Nat Chem*. 2012;4(4):310–316. doi:10.1038/nchem.1272
18. Gu T, Cheng L, Gong F, et al. Upconversion composite nanoparticles for tumor hypoxia modulation and enhanced near-infrared-triggered photodynamic therapy. *ACS Appl Mater Interfaces*. 2018;10(18):15494–15503. doi:10.1021/acsami.8b03238
19. Zhu W, Dong Z, Fu T, et al. Modulation of hypoxia in solid tumor microenvironment with MnO2Nanoparticles to enhance photodynamic therapy. *Adv Funct Mater*. 2016;26(30):5490–5498. doi:10.1002/adfm.201600676
20. Fix SM, Borden MA, Dayton PA. Therapeutic gas delivery via microbubbles and liposomes. *J Controlled Release*. 2015;209:139–149. doi:10.1016/j.jconrel.2015.04.027
21. Zheng D-W, Li B, Li C-X, et al. Carbon-dot-decorated carbon nitride nanoparticles for enhanced photodynamic therapy against hypoxic tumor via water splitting. *ACS Nano*. 2016;10(9):8715–8722. doi:10.1021/acsnano.6b04156
22. Tang Z, Li L, Tang Y, et al. CDK2 positively regulates aerobic glycolysis by suppressing SIRT5 in gastric cancer. *Cancer Sci*. 2018;109(8):2590–2598. doi:10.1111/cas.13691
23. Kalyanaraman B, Cheng G, Hardy M, et al. A review of the basics of mitochondrial bioenergetics, metabolism, and related signaling pathways in cancer cells: therapeutic targeting of tumor mitochondria with lipophilic cationic compounds. *Redox Biol*. 2018;14:316–327. doi:10.1016/j.redox.2017.09.020
24. Song X, Feng L, Liang C, Gao M, Song G, Liu Z. Liposomes co-loaded with metformin and chlorin e6 modulate tumor hypoxia during enhanced photodynamic therapy. *Nano Res*. 2017;10(4):1200–1212. doi:10.1007/s12274-016-1274-8

25. Benej M, Hong X, Vibhute S, et al. Papaverine and its derivatives radiosensitize solid tumors by inhibiting mitochondrial metabolism. *Proc Nat Acad Sci*. 2018;115(42):10756. doi:10.1073/pnas.1808945115
26. Molina JR, Sun Y, Protopopova M, et al. An inhibitor of oxidative phosphorylation exploits cancer vulnerability. *Nat Med*. 2018;24(7):1036–1046. doi:10.1038/s41591-018-0052-4
27. Zannella VE, Dal Pra A, Muaddi H, et al. Reprogramming metabolism with metformin improves tumor oxygenation and radiotherapy response. *Clin Cancer Res*. 2013;19(24):6741. doi:10.1158/1078-0432.CCR-13-1787
28. Mo R, Gu Z. Tumor microenvironment and intracellular signal-activated nanomaterials for anticancer drug delivery. *Materials Today*. 2016;19(5):274–283. doi:10.1016/j.mattod.2015.11.025
29. Paliwal SR, Paliwal R, Vyas SP. A review of mechanistic insight and application of pH-sensitive liposomes in drug delivery. *Drug Deliv*. 2015;22(3):231–242. doi:10.3109/10717544.2014.882469
30. Lei J, Cong S, Song M, et al. Combination of doxorubicin with harmine-loaded liposomes exerting synergistic antitumor efficacy. *Drug Dev Ind Pharm*. 2018;44(4):570–581. doi:10.1080/03639045.2017.1405432
31. Zhao Y, Ren W, Zhong T, et al. Tumor-specific pH-responsive peptide-modified pH-sensitive liposomes containing doxorubicin for enhancing glioma targeting and anti-tumor activity. *J Controlled Release*. 2016;222:56–66. doi:10.1016/j.jconrel.2015.12.006
32. Li J, Zhou Y, Li C, et al. Poly(2-ethyl-2-oxazoline)–doxorubicin conjugate-based dual endosomal pH-sensitive micelles with enhanced antitumor efficacy. *Bioconjug Chem*. 2015;26(1):110–119. doi:10.1021/bc5004718
33. Cheng K, Ding Y, Zhao Y, et al. Sequentially responsive therapeutic peptide assembling nanoparticles for dual-targeted cancer immunotherapy. *Nano Lett*. 2018;18(5):3250–3258. doi:10.1021/acs.nanolett.8b01071
34. Mero A, Pasut G, Via LD, et al. Synthesis and characterization of poly(2-ethyl 2-oxazoline)-conjugates with proteins and drugs: suitable alternatives to PEG-conjugates? *J Controlled Release*. 2008;125(2):87–95. doi:10.1016/j.jconrel.2007.10.010
35. Lee SC, Lee HJ. pH-controlled, polymer-mediated assembly of polymer micelle nanoparticles. *Langmuir*. 2007;23(2):488–495. doi:10.1021/la0623580
36. Heneweer C, Gendy SEM, Peñate-Medina O. Liposomes and inorganic nanoparticles for drug delivery and cancer imaging. *Ther Deliv*. 2012;3(5):645–656. doi:10.4155/tde.12.38